

Characterization of room-temperature in-plane magnetization in thin flakes of CrTe₂ with a single spin magnetometer

F. Fabre,¹ A. Finco,¹ A. Purbawati,² A. Hadj-Azzem,² N. Rougemaille,² J. Coraux,² I. Philip,¹ and V. Jacques¹

¹Laboratoire Charles Coulomb, Université de Montpellier and CNRS, 34095 Montpellier, France

²Univ. Grenoble Alpes, CNRS, Grenoble INP, Institut NEEL, 38000 Grenoble, France

(Dated: May 2, 2022)

We demonstrate room-temperature ferromagnetism with in-plane magnetic anisotropy in thin flakes of the CrTe₂ van der Waals ferromagnet. Using quantitative magnetic imaging with a single spin magnetometer based on a nitrogen-vacancy defect in diamond, we infer a room-temperature in-plane magnetization in the range of $M \sim 25$ kA/m for flakes with thicknesses down to 20 nm. These results make CrTe₂ a unique system in the growing family of van der Waals ferromagnets, because it is the only material platform known to date which offers an intrinsic in-plane magnetization and a Curie temperature above 300 K in thin flakes.

Ferromagnetic van der Waals (vdW) crystals offer numerous opportunities both for the study of exotic magnetic phase transitions in low-dimensional systems [1] and for the design of innovative, atomically-thin spintronic devices [2, 3]. Since the discovery of a two-dimensional (2D) magnetic order in monolayers of CrI₃ [4] and Cr₂Ge₂Te₆ [5] crystals, the family of vdW ferromagnets has expanded very rapidly [6–8]. However, most of these compounds have a Curie temperature (T_c) well below 300 K, which appears as an important drawback for future technological applications. An intense research effort is therefore currently devoted to the identification of high- T_c 2D magnets [3].

In this context, the vdW crystal Fe₃GeTe₂ appears as a serious candidate because it can be grown in wafer-scale through molecular beam epitaxy and it exhibits a strong perpendicular magnetic anisotropy [9, 10]. Although its intrinsic T_c drops to 130 K in the monolayer limit [11], it can be raised above room-temperature either by ionic gating [12], micro-patterning [13], interfacial engineering [14] or by varying the composition of the iron-based Fe_xGeTe₂ alloy [15, 16]. Another promising strategy consists in incorporating magnetic dopants into 2D materials to form diluted magnetic semiconductors [17]. This approach was recently employed to induce room-temperature ferromagnetism in WSe₂ monolayers doped with vanadium [18, 19]. Finally, an intrinsic ferromagnetic order was reported in epitaxial layers of VSe₂ [20], MnSe₂ [21] and VTe₂ [22] under ambient conditions, although the interpretation of these experiments still remains debated [23, 24].

In this work, we follow an alternative research direction by studying the room-temperature magnetic properties of micron-sized flakes exfoliated from a CrTe₂ crystal with 1T structure. In its bulk form, this layered transition metal dichalcogenide is a ferromagnet with *in-plane* magnetization, *i.e.* pointing perpendicular to the c axis, and a T_c around 320 K [25]. This combination of properties is unique in the growing family of vdW ferromagnets. Recent studies have reported that the magnetic order is

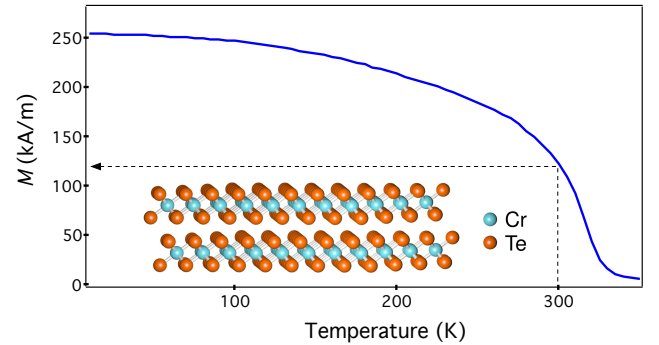


FIG. 1. Temperature dependence of the magnetization M in a bulk crystal of CrTe₂ with 1T polytype. The measurement is performed by vibrating sample magnetometry under a magnetic field of 500 mT. At room temperature, the magnetization is around 120 kA/m (black dashed lines). The inset shows the layered crystal structure of 1T-CrTe₂.

preserved at room temperature in exfoliated CrTe₂ flakes with thicknesses in the range of a few tens of nanometers [26, 27]. However, obtaining quantitative estimates of the magnetization in such micron-sized flakes remains a difficult task, which requires the use of non-invasive magnetic microscopy techniques combining high sensitivity with high spatial resolution. These performances are offered by magnetometers employing a single nitrogen-vacancy (NV) defect in diamond as an atomic-size quantum sensor [28–30]. In recent years, this microscopy technique has found many applications in condensed matter physics [31], including the study of chiral spin textures in ultrathin magnetic materials [32–34], current flow imaging in graphene [35] and the analysis of the magnetic order in vdW magnets down to the monolayer limit [36–38]. Here we use scanning-NV magnetometry to infer quantitatively the in-plane magnetization in exfoliated CrTe₂ flakes under ambient conditions. Our measurements confirm that the ferromagnetic order is preserved in few tens of nanometers thick flakes, although with a low room-temperature magnetization $M \sim 25$ kA/m. This value

is five times smaller than the one measured in a bulk CrTe_2 crystal. Such a reduction of the magnetization is attributed to a decreased Curie temperature in exfoliated flakes.

A bulk $1T\text{-CrTe}_2$ crystal was synthesized following the procedure described in Ref. [25]. The in-plane magnetization of this layered ferromagnet was first characterized as a function of temperature through vibrating sample magnetometry under a magnetic field of 500 mT. The results shown in Fig. 1 indicate a Curie temperature around 320 K and a magnetization reaching $M \sim 120$ kA/m under ambient conditions. CrTe_2 flakes with thicknesses ranging from a few tens to a hundred of nanometers were then obtained by mechanical exfoliation and transferred on a SiO_2/Si substrate. We note that the probability to obtain thin CrTe_2 flakes through mechanical exfoliation is still very low compared to other layered transition metal dichalcogenides, such as MoS_2 or WSe_2 [27]. The thinnest flake studied in this work has a thickness of ~ 20 nm. Like all van der Waals ferromagnets known to date, CrTe_2 flakes are unstable under oxygen atmosphere. However, a recent study combining X-ray and Raman spectroscopy has shown that oxidation of CrTe_2 flakes occurs typically within a day scale under ambient conditions and is limited to the very first outer layers [27]. In this work, CrTe_2 flakes were not encapsulated and all the measurements were done within a day after exfoliation to mitigate oxidation.

Magnetic imaging was performed with a scanning-NV magnetometer operating under ambient conditions [30]. As sketched in Fig. 2(a), a single NV defect integrated into the tip of an atomic force microscope (AFM) was scanned above CrTe_2 flakes to probe their stray magnetic fields. At each point of the scan, a confocal optical microscope placed above the tip was used to monitor the magnetic-field-dependent photoluminescence (PL) properties of the NV defect under green laser illumination. In this work, we employed a commercial diamond tip (Qnami, Quantilever MX) with a characteristic NV-to-sample distance $d_{\text{NV}} = 80 \pm 10$ nm, as measured through an independent calibration procedure [39]. Two different magnetic imaging modes were used. In the limit of weak stray fields (< 5 mT), quantitative magnetic field mapping was obtained by recording the Zeeman shift of the NV defect electron spin sublevels through optical detection of the electron spin resonance (ESR). This method relies on microwave driving of the NV spin transition combined with the detection of the spin-dependent PL intensity of the NV defect [40]. For stronger magnetic fields (> 5 mT), the scanning-NV magnetometer was rather used in all-optical, PL quenching mode [41, 42]. In this case, localized regions of the sample producing large stray fields are simply revealed by an overall decrease of the PL signal induced by a mixing of the NV defect spin sublevels [43]. We note that the diameter of the scanning diamond tip is around 200 nm in order to

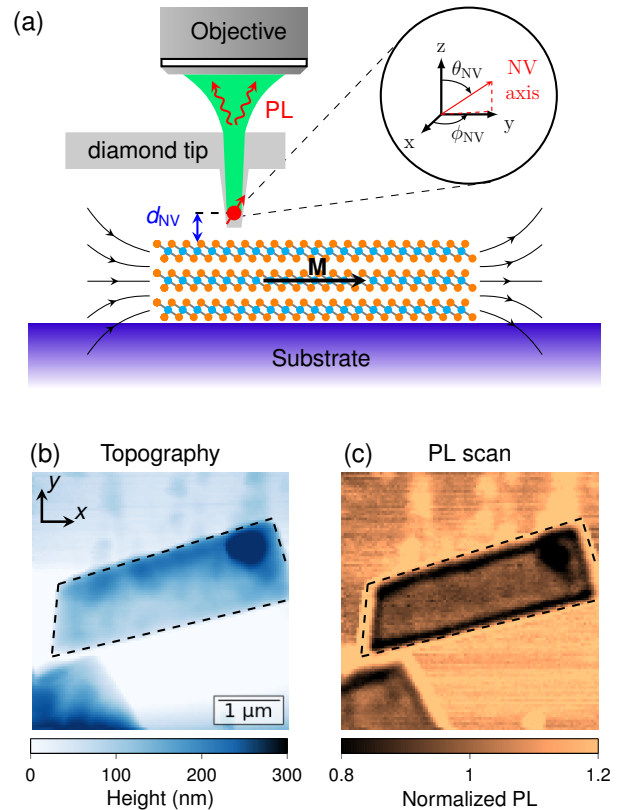


FIG. 2. (a) Principle of the experiment. A single NV defect (red arrow) localized at the apex of a diamond tip is scanned above CrTe_2 flakes. A microscope objective placed above the tip is used to collect the photoluminescence (PL) of the NV defect under green laser excitation. In this work, the NV-to-sample distance is $d_{\text{NV}} \sim 80$ nm and the quantization axis of the NV defect is characterized by the spherical angles ($\theta_{\text{NV}} = 58^\circ$, $\phi_{\text{NV}} = 103^\circ$) in the laboratory frame of reference (x, y, z). The black arrows indicate the magnetic field lines generated at the edges of a CrTe_2 flake with uniform in-plane magnetization \mathbf{M} . (b) AFM image of a 150 nm-thick CrTe_2 flake. (c) Corresponding PL map showing a quenching contour at the edges of the flake with a contrast around 20%. The shape of the flake is indicated by the black dashed lines.

act as an efficient waveguide for the PL emission of the NV defect [44, 45]. Consequently, such tips cannot provide precise topographic information of the sample. For the thinnest flakes, the topography was thus imaged by using conventional, sharp AFM tips.

In a first experiment, we imaged a CrTe_2 flake with a large thickness $t \sim 150$ nm [Fig. 2(b)]. For a uniformly magnetized flake, stray magnetic fields are produced at the edges of the flake, as sketched in Fig. 2(a). Considering the saturation magnetization of the bulk CrTe_2 crystal, magnetic simulations predict a stray field amplitude larger than 10 mT at a distance $d_{\text{NV}} \sim 80$ nm above the edges of the 150-nm-thick flake. The scanning-NV magnetometer was thus operated in the PL quenching mode for such a thick flake. Fig. 2(c) displays the resulting PL

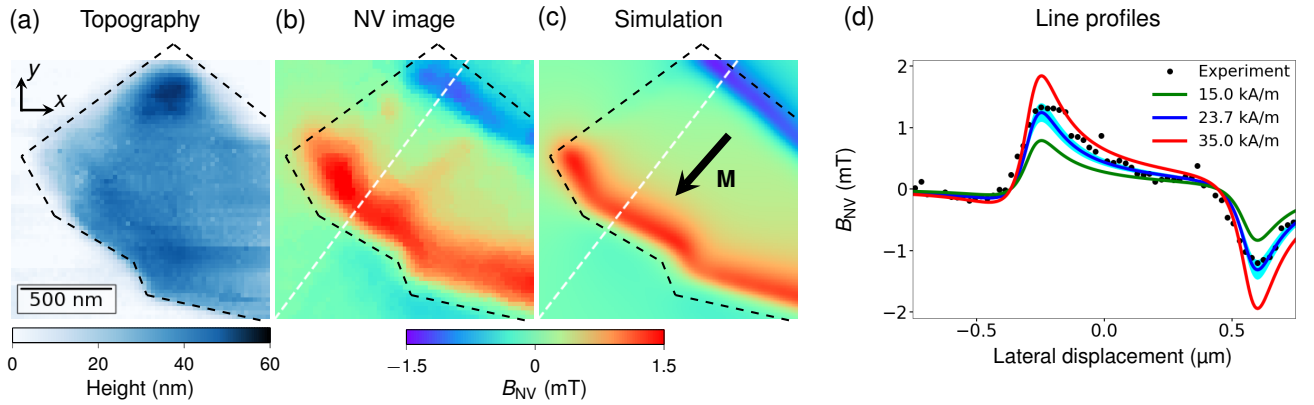


FIG. 3. (a) AFM image of a 40 nm-thick CrTe₂ flake recorded with the scanning-NV microscope. (b) Simultaneously recorded distribution of the magnetic field component B_{NV} . For this measurement, a bias field of 3 mT is applied along the NV defect axis in order to infer the sign of the stray magnetic field [30]. (c) Simulated magnetic field distribution B_{NV} for a uniform in-plane magnetization \mathbf{M} (black arrow) with an azimuthal angle $\phi_M = -135^\circ$ in the (x, y) plane and a norm $M = 23.7$ kA/m. The calculation is done at a distance $d_{NV} = 80$ nm above the flake, whose shape is extracted from the topography image [black dashed lined in (a)]. (d) Fitting of an experimental line profile (black markers) with the magnetic calculation (blue solid line). The position of the linecuts are indicated by the white dashed lines in (b) and (c). A magnetization $M = 23.7 \pm 2.8$ kA/m is obtained, the uncertainty being illustrated by the blue shaded area. The red and green solid lines indicate the result of the calculation for $M = 35$ kA/m and $M = 15$ kA/m, respectively.

map, which is characterized by a strong quenching at the edges of the flake, as expected for a single ferromagnetic domain. Although qualitative, this preliminary experiment confirms that mechanical exfoliation preserves the ferromagnetic order in CrTe₂ under ambient conditions.

Thinner CrTe₂ flakes, *i.e.* producing less stray field, were then studied through quantitative magnetic field imaging. To this end, a microwave excitation was applied through a copper microwire directly spanned on the sample surface and the Zeeman shift of the NV defect's ESR frequency was recorded at each point of the scan. In the weak field regime, the ESR frequency is shifted linearly with the projection B_{NV} of the stray magnetic field along the NV defect quantization axis [30]. This axis was precisely measured by applying a calibrated magnetic field [46], leading to the spherical angles $\theta_{NV} = 58^\circ$ and $\phi_{NV} = 103^\circ$ in the laboratory frame (x, y, z) , as illustrated in Fig. 2(a).

A map of B_{NV} recorded above a 40-nm thick CrTe₂ flake is shown in Fig. 3(b). A stray magnetic field around ± 1.5 mT is detected at two opposite edges of the flake. In principle, the underlying sample magnetization can be retrieved from such a quantitative magnetic field map by using reverse propagation methods with well-adjusted filters in Fourier-space [31]. Under several assumptions, this method can be quite robust for magnetic materials with out-of-plane magnetization [36–38]. For in plane magnets, however, the reconstruction procedure amplifies noise and is thus much less efficient [47]. As a result, the recorded magnetic field distribution was rather compared to magnetic calculations in order to extract quantitative information on the sample magnetization.

The geometry of the flake used for the calculation was inferred from the AFM image simultaneously recorded with the NV microscope [Fig. 3(a)]. Assuming a uniform in-plane magnetization \mathbf{M} with an azimuthal angle ϕ_M in the (x, y) plane, the stray field was calculated at a distance d_{NV} above the flake and then projected along the NV quantization axis in order to simulate a map of B_{NV} . By comparing experimental data with magnetic maps simulated for different values of the angle ϕ_M , the orientation of the in-plane magnetization was first identified, leading to $\phi_M = -135 \pm 5^\circ$, *i.e.* pointing along the short axis of the flake [Fig. 3(c)]. This result suggests the presence of a non-negligible magnetocrystalline anisotropy, in agreement with recent works [27]. Indeed, considering only the shape anisotropy should promote an in-plane magnetization pointing along the long axis of the flake. The norm M of the magnetization vector was then estimated by fitting experimental line profiles with the result of the calculation, leading to $M = 23.7 \pm 2.8$ kA/m [Fig. 3(d)]. We note that the stray field amplitude depends on several parameters including d_{NV} , ϕ_M , the flake thickness t and the NV defect quantization axis (θ_{NV} , ϕ_{NV}). Any imprecisions on these parameters directly translate into uncertainties on the evaluation of the magnetization M . The uncertainties were analyzed following the procedure described in Ref. [48]. An overall uncertainty $\epsilon \sim 12\%$ was obtained, which mainly results from the imperfect knowledge of the NV-to-sample distance d_{NV} in this experiment.

The room-temperature magnetization measured in the exfoliated CrTe₂ flake is almost five times smaller than the one obtained in the bulk crystal. This observation

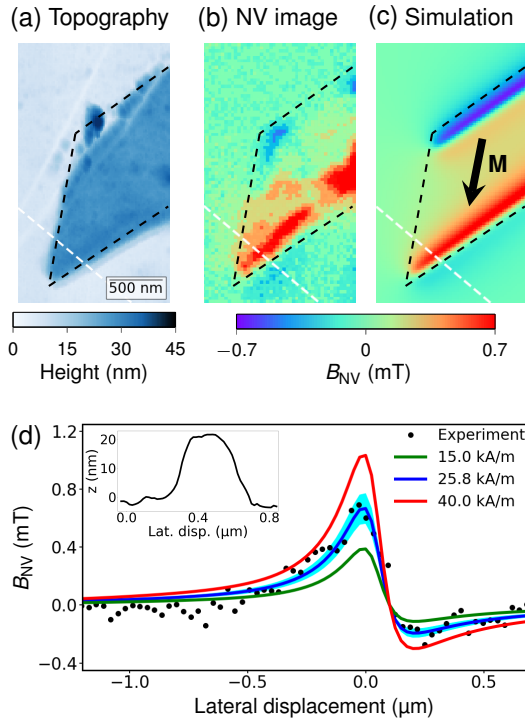


FIG. 4. (a) AFM image of a 20-nm thick CrTe_2 flake. (b) Corresponding map of the magnetic field component B_{NV} . (c) Simulated map of B_{NV} for a uniform in-plane magnetization \mathbf{M} (black arrow) with an azimuthal angle $\phi_M = -100^\circ$ in the (x, y) plane and a norm $M = 25.8 \text{ kA/m}$. The black dashed line indicate the shape of the flake used for the simulation. (d) Fitting of an experimental line profile (black markers) with the magnetic simulation (blue solid line). The linecuts are indicated by the white dashed lines in (b) and (c). A magnetization $M = 25.8 \pm 4.0 \text{ kA/m}$ is obtained, the uncertainty being illustrated by the blue shaded area. The inset shows a linecut across the flake (white dashed lines in (a)).

could be explained by a degradation of the sample surface through oxidation processes, leading to a thinner effective magnetic thickness. However, recent experiments relying on X-ray magnetic circular dichroism coupled to photoemission electron microscopy (XMCD-PEEM) have shown that oxidation is limited to the first outer layers of the CrTe_2 flake [27]. Considering a 40-nm thick CrTe_2 flake, surface oxidation can thus be safely neglected, and cannot explain the observed reduction of the magnetization. This effect rather results from a decrease of the Curie temperature in exfoliated flakes, a phenomenon commonly observed in thin vdW magnets [26]. The decreased magnetization observed in CrTe_2 flakes would correspond to a reduction of T_c by about 20 K.

To support this finding, a similar analysis was performed for a 20-nm thick flake [Fig. 4(a)]. Here, the topography of the flake was recorded by using a conventional AFM tip in order to obtain more precise measurements. The corresponding magnetic field distribution is

shown in Fig. 4(b). A stray magnetic field is mainly detected along the bottom edge of the flake. On the opposite edge, the stray field distribution is quite inhomogeneous. This observation is attributed to damages of the flake that can be observed in the AFM image. A simulation of the stray field distribution for a magnetization with an azimuthal angle $\phi_M = -100 \pm 10^\circ$ reproduces fairly well the experimental results [Fig. 4(c)] and a quantitative analysis of line profiles across the bottom edge of the flake leads to $M = 25.8 \pm 4.0 \text{ kA/m}$ [Fig. 4(d)], a similar value to that obtained in the 40-nm thick flake. This observation indicates that the magnetization is not significantly modified for thicknesses lying in the few tens of nanometers range.

To conclude, we have used quantitative magnetic imaging with a scanning-NV magnetometer to demonstrate that exfoliated CrTe_2 flakes with thicknesses down to 20 nm exhibit an in-plane ferromagnetic order at room temperature with a typical magnetization in the range of $M \sim 25 \text{ kA/m}$. These results make CrTe_2 a unique system in the growing family of vdW ferromagnets, because it is the only material platform known to date which offers an intrinsic in-plane magnetization and a T_c above room temperature in thin flakes. These properties might offer several opportunities for studying magnetic phase transition in 2D-XY systems [49] and to design spintronic devices based on vdW magnets. The next challenge will be to assess if the ferromagnetic order is preserved at room temperature in the few layers limit.

Acknowledgements: The authors warmly thank J. Vogel and M. Núñez-Regueiro for fruitful discussions. This research has received funding from the European Union H2020 Program under Grant Agreement No. 820394 (ASTERIQs), the DARPA TEE program, and the Flag-ERA JTC 2017 project MORE-MXenes. A.F. acknowledges financial support from the EU Horizon 2020 Research and Innovation program under the Marie Skłodowska-Curie Grant Agreement No. 846597 (DI-MAF).

-
- [1] J. M. Kosterlitz and D. J. Thouless, *J. Phys. C: Solid State Phys.* **6**, 1181 (1973).
 - [2] H. Li, S. Ruan, and Y.-J. Zeng, *Adv. Mater.* **31**, 1900065 (2019).
 - [3] M.-C. Wang, C.-C. Huang, C.-H. Cheung, C.-Y. Chen, S. G. Tan, T.-W. Huang, Y. Zhao, Y. Zhao, G. Wu, Y.-P. Feng, H.-C. Wu, and C.-R. Chang, *Annalen der Physik* **532**, 1900452 (2020).
 - [4] B. Huang, G. Clark, E. Navarro-Moratalla, D. R. Klein, R. Cheng, K. L. Seyler, D. Zhong, E. Schmidgall, M. A. McGuire, D. H. Cobden, W. Yao, D. Xiao, P. Jarillo-Herrero, and X. Xu, *Nature* **546**, 270 (2017).
 - [5] C. Gong, L. Li, Z. Li, H. Ji, A. Stern, Y. Xia, T. Cao, W. Bao, C. Wang, Y. Wang, Z. Q. Qiu, R. J. Cava, S. G.

- Louie, J. Xia, and X. Zhang, *Nature* **546**, 265 (2017).
- [6] K. S. Burch, D. Mandrus, and J.-G. Park, *Nature* **563**, 47 (2018).
- [7] C. Gong and X. Zang, *Science* **363** (2019).
- [8] M. Gibertini, M. Koperski, A. F. Morpurgo, and K. S. Novoselov, *Nature Nanotechnology* **14**, 408 (2019).
- [9] S. Liu, X. Yuan, Y. Zou, Y. Sheng, C. Huang, E. Zhang, J. Ling, Y. Liu, W. Wang, C. Zhang, J. Zou, K. Wang, and F. Xiu, *npj 2D Materials and Applications* **1**, 30 (2017).
- [10] N. Leon-Brito, E. D. Bauer, F. Ronning, J. D. Thompson, and R. Movshovich, *Journal of Applied Physics* **120**, 083903 (2016).
- [11] Z. Fei, B. Huang, P. Malinowski, W. Wang, T. Song, J. Sanchez, W. Yao, D. Xiao, X. Zhu, A. F. May, W. Wu, D. H. Cobden, J.-H. Chu, and X. Xu, *Nature Materials* **17**, 778 (2018).
- [12] Y. Deng, Y. Yu, Y. Song, J. Zhang, N. Z. Wang, Z. Sun, Y. Yi, Y. Z. Wu, S. Wu, J. Zhu, J. Wang, X. H. Chen, and Y. Zhang, *Nature* **563**, 94 (2018).
- [13] Q. Li, M. Yang, C. Gong, R. V. Chopdekar, A. T. N'Diaye, J. Turner, G. Chen, A. Scholl, P. Shafer, E. Arenholz, A. K. Schmid, S. Wang, K. Liu, N. Gao, A. S. Admasu, S.-W. Cheong, C. Hwang, J. Li, F. Wang, X. Zhang, and Z. Qiu, *Nano Lett.* **18**, 5974 (2018).
- [14] H. Wang, Y. Liu, P. Wu, W. Hou, Y. Jiang, X. Li, C. Pandey, D. Chen, Q. Yang, H. Wang, D. Wei, N. Lei, W. Kang, L. Wen, T. Nie, W. Zhao, and K. L. Wang, *ACS Nano* **14**, 10045 (2020).
- [15] A. F. May, D. Ovchinnikov, Q. Zheng, R. Hermann, S. Calder, B. Huang, Z. Fei, Y. Liu, X. Xu, and M. A. McGuire, *ACS Nano* **13**, 4436 (2019).
- [16] J. Seo, D. Y. Kim, E. S. An, K. Kim, G.-Y. Kim, S.-Y. Hwang, D. W. Kim, B. G. Jang, H. Kim, G. Eom, S. Y. Seo, R. Stania, M. Muntwiler, J. Lee, K. Watanabe, T. Taniguchi, Y. J. Jo, J. Lee, B. I. Min, M. H. Jo, H. W. Yeom, S.-Y. Choi, J. H. Shim, and J. S. Kim, *Science Advances* **6** (2020).
- [17] P. Mallet, F. Chiappello, H. Okuno, H. Boukari, M. Jamet, and J.-Y. Veuillen, *Phys. Rev. Lett.* **125**, 036802 (2020).
- [18] S. J. Yun, D. L. Duong, D. M. Ha, K. Singh, T. L. Phan, W. Choi, Y.-M. Kim, and Y. H. Lee, *Advanced Science* **7**, 1903076 (2020).
- [19] Z. F., B. Zheng, A. Sebastian, H. Olson, M. Liu, K. Fujisawa, Y. T. H. Pham, V. Ortiz Jimenez, V. Kalappattil, L. Miao, T. Zhang, R. Pendurthi, Y. Lei, A. L. Elias, Y. Wang, N. Alem, P. E. Hopkins, S. Das, V. H. Crespi, M.-H. Phan, and M. Terrones, *arXiv:2005.01965* (2020).
- [20] M. Bonilla, S. Kolekar, Y. Ma, H. C. Diaz, V. Kalappattil, R. Das, T. Eggers, H. R. Gutierrez, M.-H. Phan, and M. Batzill, *Nature Nanotechnology* **13**, 289 (2018).
- [21] D. J. O'Hara, T. Zhu, A. H. Trout, A. S. Ahmed, Y. K. Luo, C. H. Lee, M. R. Brenner, S. Rajan, J. A. Gupta, D. W. McComb, and R. K. Kawakami, *Nano Letters* **18**, 3125 (2018).
- [22] J. Li, B. Zhao, P. Chen, R. Wu, B. Li, Q. Xia, G. Guo, J. Luo, K. Zang, Z. Zhang, H. Ma, G. Sun, X. Duan, and X. Duan, *Advanced Materials* **30**, 1801043 (2018).
- [23] J. Feng, D. Biswas, A. Rajan, M. D. Watson, F. Mazzola, O. J. Clark, K. Underwood, I. Markovic, M. McLaren, A. Hunter, D. M. Burn, L. B. Duffy, S. Barua, G. Balakrishnan, F. Bertran, P. Le Fevre, T. K. Kim, G. van der Laan, T. Hesjedal, P. Wahl, and P. D. C. King, *Nano Lett.* **18**, 4493 (2019).
- [24] P. K. J. Wong, W. Zhang, F. Bussolotti, X. Yin, T. S. Herng, L. Zhang, Y. L. Huang, G. Vinai, S. Krishnamurthi, D. W. Bukhvalov, Y. J. Zheng, R. Chua, A. T. N'Diaye, S. A. Morton, C.-Y. Yang, K.-H. Ou Yang, P. Torelli, W. Chen, K. E. J. Goh, J. Ding, M.-T. Lin, G. Brocks, M. P. de Jong, A. H. Castro Neto, and A. T. S. Wee, *Advanced Materials* **31**, 1901185 (2019).
- [25] D. C. Freitas, R. Weht, A. Sulpice, G. Remenyi, P. Strobel, F. Gay, J. Marcus, and M. Núñez-Regueiro, *Journal of Physics: Condensed Matter* **27**, 176002 (2015).
- [26] X. Sun, W. Li, X. Wang, Q. Sui, T. Zhang, Z. Wang, L. Liu, D. Li, S. Feng, S. Zhong, H. Wang, V. Bouchiat, M. Nunez Regueiro, N. Rougemaille, J. Coraux, A. Purbawati, A. Hadj-Azzem, Z. Wang, B. Dong, X. Wu, T. Yang, G. Yu, B. Wang, Z. Han, X. Han, and Z. Zhang, *Nano Research* (2020).
- [27] A. Purbawati, J. Coraux, J. Vogel, A. Hadj-Azzem, N. Wu, N. Bendiab, D. Jegouso, J. Renard, L. Marty, V. Bouchiat, A. Sulpice, L. Aballe, M. Foerster, F. Genuzio, A. Locatelli, T. O. Menteş, Z. V. Han, X. Sun, M. Núñez-Regueiro, and N. Rougemaille, *ACS Appl. Mater. Interfaces* **12**, 30702 (2020).
- [28] G. Balasubramanian, I. Y. Chan, R. Kolesov, M. Al-Hmoud, J. Tisler, C. Shin, C. Kim, A. Wojcik, P. R. Hemmer, A. Krueger, T. Hanke, A. Leitenstorfer, R. Bratschitsch, F. Jelezko, and J. Wrachtrup, *Nature* **455**, 648 (2008).
- [29] J. R. Maze, P. L. Stanwix, J. S. Hodges, S. Hong, J. M. Taylor, P. Cappellaro, L. Jiang, M. V. G. Dutt, E. Togan, A. S. Zibrov, A. Yacoby, R. L. Walsworth, and M. D. Lukin, *Nature* **455**, 644 (2008).
- [30] L. Rondin, J.-P. Tetienne, T. Hingant, J.-F. Roch, P. Maletinsky, and V. Jacques, *Reports on Progress in Physics* **77**, 056503 (2014).
- [31] F. Casola, T. van der Sar, and A. Yacoby, *Nature Reviews Materials* **3**, 17088 (2018).
- [32] J.-P. Tetienne, T. Hingant, L. J. Martinez, S. Rohart, A. Thiaville, L. H. Diez, K. Garcia, J.-P. Adam, J.-V. Kim, J.-F. Roch, I. M. Miron, G. Gaudin, L. Vila, B. Ocker, D. Ravelosona, and V. Jacques, *Nature Communications* **6**, 6733 (2015).
- [33] Y. Dovzhenko, F. Casola, S. Schlotter, T. X. Zhou, F. Buttner, R. L. Walsworth, G. S. D. Beach, and A. Yacoby, *Nature Communications* **9**, 2712 (2018).
- [34] J.-Y. Chauleau, T. Chirac, S. Fusil, V. Garcia, W. Akhtar, J. Tranchida, P. Thibaudeau, I. Gross, C. Blouzon, A. Finco, M. Bibes, B. Dkhil, D. D. Khalyavin, P. Manuel, V. Jacques, N. Jaouen, and M. Viret, *Nature Materials* **19**, 386 (2020).
- [35] M. J. H. Ku, T. X. Zhou, Q. Li, Y. J. Shin, J. K. Shi, C. Burch, L. E. Anderson, A. T. Pierce, Y. Xie, A. Hamo, U. Vool, H. Zhang, F. Casola, T. Taniguchi, K. Watanabe, M. M. Fogler, P. Kim, A. Yacoby, and R. L. Walsworth, *Nature* **583**, 537 (2020).
- [36] L. Thiel, Z. Wang, M. A. Tschudin, D. Rohner, I. Gutiérrez-Lezama, N. Ubrig, M. Gibertini, E. Gianini, A. F. Morpurgo, and P. Maletinsky, *Science* **364**, 973 (2019).
- [37] D. A. Broadway, S. C. Scholten, C. Tan, N. Dontschuk, S. E. Lillie, B. C. Johnson, G. Zheng, Z. Wang, A. R. Oganov, S. Tian, C. Li, H. Lei, L. Wang, L. C. L. Hollenberg, and J.-P. Tetienne, *Adv. Mater.* **n/a**, 2003314 (2020).
- [38] Q.-C. Sun, T. Song, E. Anderson, T. Shalomayeva,

- J. Förster, A. Brunner, T. Taniguchi, K. Watanabe, J. Gräfe, R. Stöhr, X. Xu, and J. Wrachtrup, [arXiv:2009.13440](#) (2020).
- [39] T. Hingant, J.-P. Tetienne, L. J. Martínez, K. Garcia, D. Ravelosona, J.-F. Roch, and V. Jacques, *Physical Review Applied* **4**, 014003 (2015).
- [40] A. Gruber, A. Dräbenstedt, C. Tietz, L. Fleury, J. Wrachtrup, and C. V. Borczykowski, *Science* **276**, 2012 (1997).
- [41] I. Gross, W. Akhtar, A. Hrabec, J. Sampaio, L. J. Martínez, S. Chouaieb, B. J. Shields, P. Maletinsky, A. Thiaville, S. Rohart, and V. Jacques, *Phys. Rev. Materials* **2**, 024406 (2018).
- [42] W. Akhtar, A. Hrabec, S. Chouaieb, A. Haykal, I. Gross, M. Belmeguenai, M. Gabor, B. Shields, P. Maletinsky, A. Thiaville, S. Rohart, and V. Jacques, *Phys. Rev. Applied* **11**, 034066 (2019).
- [43] J.-P. Tetienne, L. Rondin, P. Spinicelli, M. Chipaux, T. Debuisschert, J.-F. Roch, and V. Jacques, *New Journal of Physics* **14**, 103033 (2012).
- [44] P. Maletinsky, S. Hong, M. S. Grinolds, B. Hausmann, M. D. Lukin, R. L. Walsworth, M. Loncar, and A. Yacoby, *Nature Nanotechnology* **7**, 320 (2012).
- [45] P. Appel, E. Neu, M. Ganzhorn, A. Barfuss, M. Batzer, M. Gratz, A. Tschöpe, and P. Maletinsky, *Review of Scientific Instruments* **87**, 063703 (2016).
- [46] L. Rondin, J.-P. Tetienne, S. Rohart, a. Thiaville, T. Hingant, P. Spinicelli, J.-F. Roch, and V. Jacques, *Nat. Commun.* **4**, 2279 (2013).
- [47] D. A. Broadway, S. E. Lillie, S. C. Scholten, D. Rohner, N. Dontschuk, P. Maletinsky, J.-P. Tetienne, and L. C. L. Hollenberg, *Phys. Rev. Applied* **14**, 024076 (2020).
- [48] I. Gross, W. Akhtar, V. Garcia, L. J. Martínez, S. Chouaieb, K. Garcia, C. Carrétéro, A. Barthélémy, P. Appel, P. Maletinsky, J.-V. Kim, J. Y. Chauleau, N. Jaouen, M. Viret, M. Bibes, S. Fusil, and V. Jacques, *Nature* **549**, 252 (2017).
- [49] A. Bedoya-Pinto, J.-R. Ji, A. Pandeya, P. Gargiani, M. Valvidares, P. Sessi, F. Radu, K. Chang, and S. Parkin, [arXiv:2006.07605](#) (2020).